THE EFFECTS OF ROLLING RESISTANCE ON THE STRESS-STRAIN AND STRAIN LOCALIZATION BEHAVIOR OF GRANULAR MATERIALS DUE TO SIMPLE SHEAR LOADING CONDITIONS.

Abdalsalam M. Muftah* and Marte S. Gutierrez†

Colorado School of Mines/Division of Engineering (CSM)
1610 Illinois St., BB 269. Golden, CO 80401, USA
*Corresponding author (e-mail: amuftah@mines.edu)

Keywords : Discrete Element Modeling, Granular materials, Rolling Resistance, Strain Localization

1 INTRODUCTION

The previous studies has conclusively shown that rolling resistance is a significant parameter influencing the stress-strain and strain localization response of granular materials when a failure state can be reached in biaxial test with small strain, (2-4%) of axial strain [1, 2]. However, in order to allow for larger deformations, numerical experiments are carried out for a simple shear test. In these simulations strain localization can be obtained for relatively high shear strain. The main objective of this paper is to present the results of a comprehensive study using DEM modeling of the effects of the variation in rolling resistance on the elasticity, shear strength, dilation and bifurcation response of granular materials subjected to simple shear loading. A comprehensive parametric study is performed whereby the magnitude of rolling resistance is varied within its full range of possible values in conjunction with variations in other model parameters, and more practically to interpret the macroscopic behavior of granular specimens subjected to different loading conditions from the viewpoint of micromechanics.

To this end, a DEM Model using the Particle Flow Code in two dimensions (PFC2D) is put forward to study localization phenomenon of granular material in simple shear test. A detailed analysis of this numerical test in view of microstructure of shear band, as regards the effect of the rolling resistance parameters on stress-strain, dilation, and other shear band features will be investigated. This objective of study is to take a close look at the deformation process by means of micro structural observation which may help to analyze the macro structural of shear bands.

2 DEM MODELING

The initial state of the DEM sample is performed under two-dimensional simple shear loading conditions. The simple shear model is rectangular, 0.06 m high and 0.12 m wide, and consists of an assembly of poly-dispersed disk-like particles (see Fig.1). Three ranges of particle radii were used: 0.3-0.4 mm, 0.3-0.6 mm and 0.3-0.8 mm. For these particle radii, the size of the model is deemed large enough to simulate a representative element volume of

granular material, but not too large to require extensive calculation times. The sample is contained by four frictionless walls. The top and bottom boundaries are confined by rigid platens and by the vertical normal stress σ_1. The left and right lateral walls are confined by semi-rigid walls and by the minor principal stress σ_3. The sample is first loaded isotropically during consolidation, then sheared by rotating the vertical walls at a constant angular velocity about the mid-points of the two walls, then increased the rotated velocity until the peak and post peak shear stress have been achieved. Shearing is performed under constant angular velocity $d\gamma / dt$ of 0.05 m/min and constant vertical normal stress. The vertical walls rotate towards the right direction under an angular velocity controlled condition.

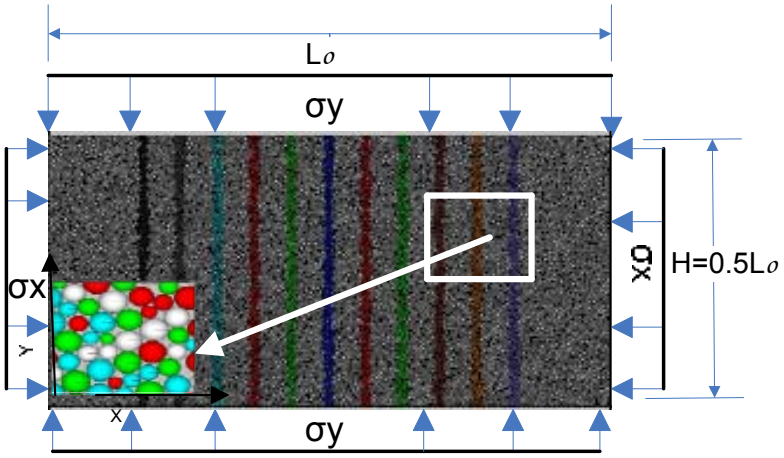

Figure1. Set-up of the simple shear DEM model for the simulation of the stress-strain and strain localization response of granular materials

The velocity of the horizontal walls is controlled automatically by a numerical servo-control program that maintains that the vertical normal stress component of the stress tensor does not change from the initial value. To generate the model, a random particle generation procedure called the "expansion method" [3] is adapted to achieve a desired sample particle size distribution and porosity. The expansion method employs a constant factor, expressed as a multiple of the particle radii, which is adjusted and the particle sizes are increased until the system reaches an equilibrium state after some calculation cycles. Due to the particle radii expansion, particles greatly overlap and thus strong repulsive forces are developed at the contacts. Cycling is required to achieve equilibrium between the unbalanced forces and the forces generated by the isotropic boundary stresses from consolidation.

The model parameters values used in the study are summarized in Table 1. The material parameters (i.e., density ρ, normal stiffness K_n and friction coefficient μ) are similar to those used by [4] in the DEM simulation of the stress-strain behavior of granular materials. Some of the parameters were given a range of values to test the sensitivity of model response to changes in parameter values. The lateral walls were given a stiffness that is $1/10^{th}$ of the particle-to-particle contact stiffness in order to simulate a semi-rigid confining membrane. The simple shear tests were run for range of vertical normal stress with σ_1 varying from 0.1 to 2 MPa. It is known in the literature that a DEM model with more than 5000 particles provides a representative element volume for the modeling of the stress-strain response of granular

materials. In this study, the number of randomly generated particles ranged from 6556 to 16190 (see Table 1).

Table 1: Model parameter values used in the DEM simulations.

Model Parameters	Values
Sample Dimensions (cm)	Height: 6, Width: 12
Particles Sizes (mm)	$0.3-0.4, 0.3-0.6, 0.3-0.$
Number of Particles	$16190, 9794, 6556$
Porosity, n	$0.10, 0.13, 0.16$
Particle Density, ρ (kg/m^3)	2630
Inter-particle Friction Coefficient, μ	$0.5, 0.6, 0.7$
Contact Normal Stiffness, $K_n(N/m)$	5×10^8.
Ratio of Shear and Normal Stiffnesses, K_s/K_n	1.0
Wall Stiffness, K_w (N/m)	5×10^7
Particle Rolling Resistance, α	$0.0, 0.01, 0.1, 0.5, 1.0$
Confining Stress, σ_1 (MPa)	$0.1, 0.8, 2.0$

The rolling resistance parameter α is affected by the particle shape, normal stiffness and normal force at a point of contact and its value typically ranges from 0 to 1. For α=0, no rolling resistance (i.e., free rolling) exists at a contact point. Based on a preliminary analysis, particle rotation is effectively prevented (i.e., no rolling) when α =1. As noted above, α is analogous to the friction coefficient μ and, thus, a value of α =1 is equivalent to prescribing a high rolling friction angle of 45°. Therefore, parameter α is given values between 0 and 1 in the simulations presented below. Table 1 lists the specific values of α in conjunction with the other model parameters used in the simulations.

3 STRAIN TENSOR AND MESH-FREE METHOD

To quantify strain localization and shear banding behavior and calculating shear strain distribution inside the shear box. A new simple method of strain calculation has been developed by [5], and used in this study to generate strain field inside a simulated simple shear box. A modified mesh-free method calculates the displacement gradient directly based on movements of individual particles. This method accounts for particle rotation and captures strain localization features at high resolution. For the current problem involving large strain localization inside the granular medium, the Green-St Venant strain tensor E_{ij} can be expressed as:

$$E_{ij} = \frac{1}{2}\left(u_{ij} + u_{ji} + u_{ij}u_{ji}\right) \quad (1)$$

Where u_{ij} is the displacement gradient tensor. It is based on the deformation measure related to the reference configuration. For peak or pre-peak shear deformation involving slight degree of strain localization, the second-order term in Eq. 1 can be neglected with little error, and the small tensor e_{ij} is computed by:

$$E_{ij} = \frac{1}{2}\left(u_{ij} + u_{ji}\right) \tag{2}$$

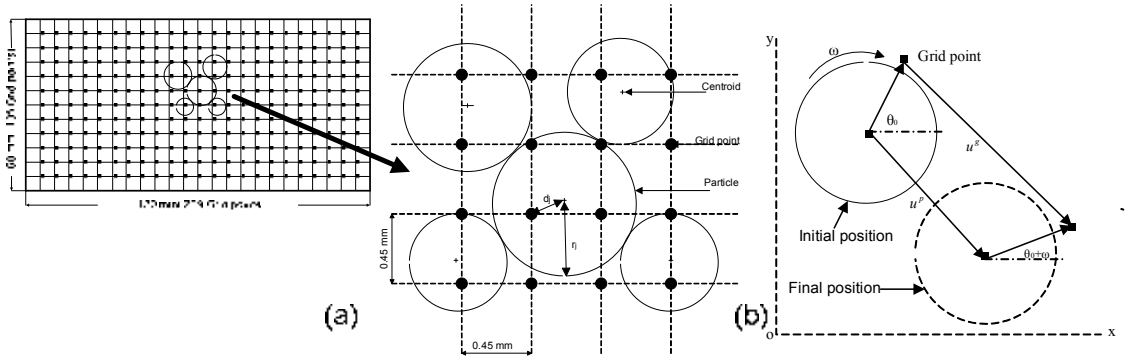

Figure 2 Schematic diagram of the mesh-free method: (a) association of a grid point with a certain particle; (b) displacement of grid point and its associated particle (Wang et al. 2007)

The mesh-free method used in this study employs a grid-type discretisation over the reference configuration. The spacing between adjacent grid points used in this study is 0.45 mm in the horizontal direction and 0.45 mm in vertical direction. As a general guide, a grid spacing of the median particle diameter D_{50} is sufficient to capture the shear localization at satisfactory resolution. A diagram of the approach is given in Fig. 2 where a rectangular grid is superimposed over the volume of particles prior to any deformation and serves as the continuum reference space. Then each grid point in the reference space is assigned to an individual particle J that has the property.

$$\frac{d_j}{r_j} \leq \frac{d_i}{r_i} \qquad \left(i = 1,2 \ldots \ldots N_p\right) i \neq j \tag{3}$$

Where r_j is the radius of particle i, d_i is the distance between the grid point and the centroid of particle i; and N_p is the total number of particles within the volume (see Fig. 2a). If the ratio of the distance between the particle centroid and its associated grid point to the particle radius is the least among all the particles, then the grid point is considered a point on the rigid or extended body of the particle. In fact, any point (not necessarily the grid point) inside the volume can be assigned to a particular particle using Eq. 3. All points that are assigned to a given single particle are then connected to form a region that belongs to this particle. Displacement of the grid point is calculated using the principal of rigid body motion of the particle.

$$\begin{pmatrix} u_x^g \\ u_y^g \end{pmatrix} = \begin{pmatrix} u_x^p \\ u_y^p \end{pmatrix} + d\begin{pmatrix} \cos(\theta_o + \omega) + \cos(\theta_o) \\ \sin(\theta_o + \omega) + \sin(\theta_o) \end{pmatrix} \tag{4}$$

Where u_x^g, u_y^g and u_x^p, u_y^p are the x and y components of displacement of grid point and particle centroid respectively; d is the distance between the grid point and the particle centroid, θ_o is the initial phase angle of the grid point position relative to the particle centroid; and ω is the accumulated rotation of the particle (see Fig. 2b). The displacement of any point inside the volume can be uniquely determined using this method; therefore a unique strain tensor is

obtained at any stage of the simulation. This method also takes into account the particle rotation; therefore it is able to capture accurately the actual strains that the granular media is experiencing.

4 RESULTS AND DISCUSSION

4.1 Effects of Rolling Resistance on Elastic Behavior

The stress-strain response of the modeled granular material subjected to simple shear loading conditions are shown in terms of the shear stress ratio τ/σ_n vs. shear strain γ_{xy} curves in Fig. 3a for different values of the rolling friction coefficient α. Except for α, all other values of the model parameters, vertical normal stresses and initial porosities are kept the same and these values are given in Table 1. It can be seen that the initial slopes of the stress-strain curves are identical for all values of α. It appears that the Young's modulus of the modeled granular material is not affected by the rolling resistance. This observation is in agreement with that of [6, 7].

Figure 3b shows the volumetric strain ε_v vs. shear strain γ_{xy} response of the modeled granular material as a function of α corresponding to the shear stress-strain response curves (see Fig. 3a). The volumetric strain increment is defined as $d\varepsilon_v = d\varepsilon_x + d\varepsilon_y$ where $d\varepsilon_y$ is the corresponding increment in the vertical dimension of the sample, which there is no change in the horizontal dimension ε_x. Like the τ/σ_n vs. γ_{xy} curves, the initial portions of the ε_v vs. γ_{xy} and τ/σ_n vs. γ_{xy} curves are very similar and are unaffected by the rolling friction coefficient. This indicates that the elastic Poisson's ratio ν of the modeled granular material is independent of α.

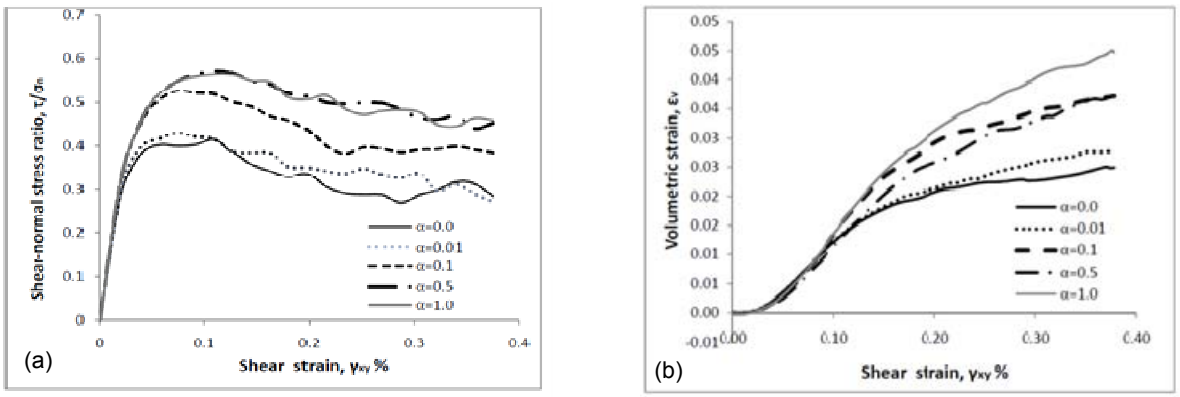

Figure 3 Effects of the rolling friction coefficient α on the (a) shear stress-strain and (b) volumetric strain response of granular materials under simple shear loading condition.

4.2 Effects of Rolling Resistance on Shear Strength and Dilatancy

In contrast to the initial state of shear stress ratio and dilatancy curves, it was found that the particle rolling resistance coefficients α played an important role in the movement of these curves of the granular specimens after bifurcation points (Figs. 3 and 4). From Fig. 3a, it can be clearly observed that an increase in the rolling friction coefficient α results in higher peak

strength. The peak shear stress ratio is increased from 0.4 to 0.57 when α is increased from 0 to 1. The increase in peak shear stress ratio with increasing α indicates that rolling resistance increases the overall frictional resistance of the granular material. The peak shear stress ratio also occurs at higher shear strains for high values of α compared to the stress-strain response at low values of α. In addition, strain softening curves show a small amount of softening in post-peak shear stress for all values ofα. It worth noting that high value of α is, small amount of softening can be increased. Figure 4a shows that the residual states are similar for granular specimens subjected to different confining stresses and the same values of α, whereas Figure 4b shows that granular specimens subjected to higher confining stress have lower volumetric dilation in volumetric strain curves.

As observed in Fig. 3b, as the shear strain is increased, the simulated materials with free rotation or with rolling resistance undergo lower volumetric contraction and start to dilate at an earlier stage with ε_1=1% compared to the materials shearing under biaxial loading condition [1]. The dilative volumetric strain increases as the rolling resistance is increased. The increased dilative volumetric changes for the models with high α-values is attributed to the fact that the increased moment between particles caused by the rolling resistance results in the particles being pushed from each other during shearing. On the other hand, in the models with low rolling resistance, the particles are free to jostle around and accommodate each other resulting in smaller dilation. Tordesillas [8] presented similar results indicating that dilatancy increases with increasing rolling resistance.

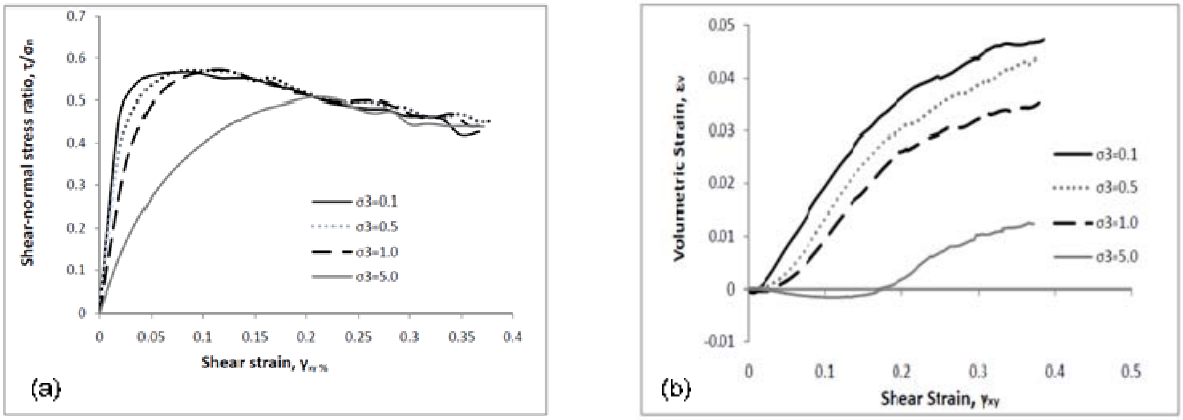

Figure 4 Effects of the vertical normal stress σ_1 on peak secant friction (a) shear stress-strain and (b) volumetric strain response of granular materials under simple shear loading condition.

Figure 5 summarizes the effects of the rolling friction coefficient α on the peak secant friction angle $\emptyset_s$, which is defined as:

$$sin(\emptyset_s) = \left(\frac{\sigma_1 - \sigma_3}{\sigma_1 + \sigma_3}\right)_{max} \tag{5}$$

For a friction coefficient of μ=0.6, the secant friction angle $\emptyset_s$ continuously increases from about 24° for α=0 to about 35° for α=1 (see Fig. 5a). The most significant increase in the secant friction angle occurs for α<0.15, and for α>0.15 the change in the friction angle is very small. The variation of the $\emptyset_s$ as function of α is similar for three values of μ: 0.5, 0.6 and 0.7. In general, for the same α-value, the peak secant friction angle increases with an increase in the

friction coefficient μ. Figure 5b shows the combined effects of α and the vertical normal stress σ_1 on the secant friction angle $\emptyset_s$.

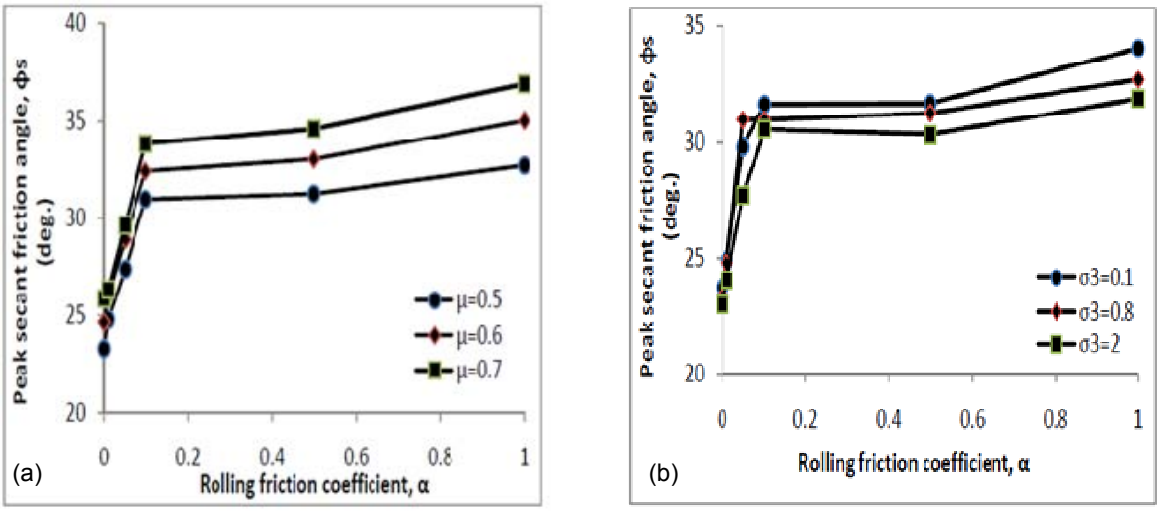

Figure 5 Effects of the rolling friction coefficient α on peak secant friction angle (a) as function of friction coefficient μ and (b) vertical normal stressσ_1.

Similar to Fig. 5a, the secant friction angle $\emptyset_s$ changes dramatically for α<0.15, and very little change occurs when α>0.15 for all σ_1-values. As expected, for the same value of α, the secant friction angle $\emptyset_s$ decreases with increasing confining stress σ_1.

Figure 6 shows the effects of rolling friction coefficient α on the peak dilation angle φ, which is defined as:

$$\sin(\varphi) = \left(\frac{d\varepsilon_1 + d\varepsilon_3}{d\varepsilon_1 - d\varepsilon_3}\right)_{max} = \frac{(d\varepsilon_v/d\varepsilon_1)_{max}}{(d\varepsilon_v/d\varepsilon_1)_{max} - 2} \quad (6)$$

In general, the dilation angle φ increases for $\alpha \leq 0.15$ then decreases afterwards. For instance, for the friction coefficient of $\mu = 0.6$, the dilation angle φ increases from its lowest value of about 12.5° for $\alpha = 0.0$ to a maximum of about 20° for $\alpha = 0.15$, then decreases to 15° for $\alpha = 1.0$. The same variation of φ with respect toα, is observed for different values of μ (Fig. 6a), and for different values of σ_1 (Fig. 6b). For the same α-value, the dilation angle increases with increasing μ (Fig. 3.6a) and decreases with increasing confining stress σ_1 (Fig. 6b).

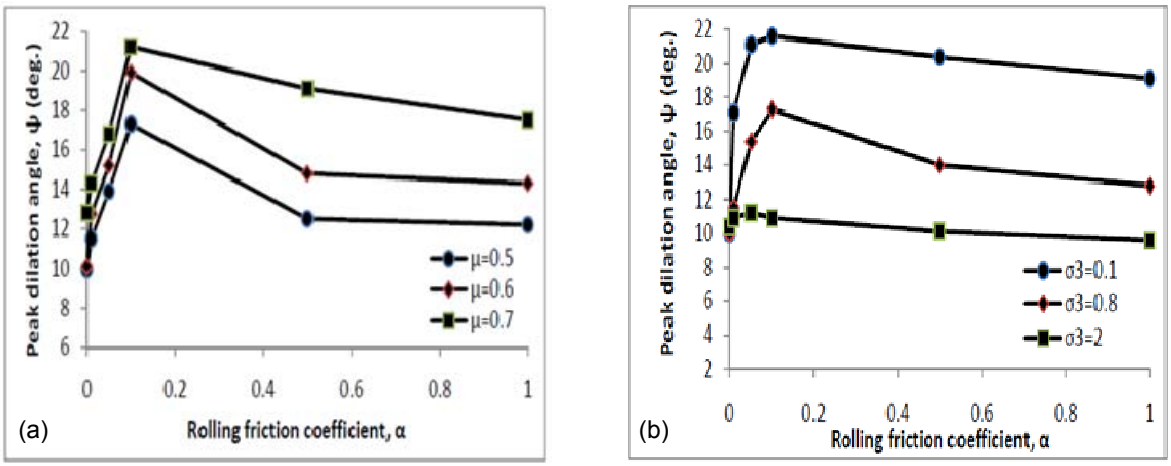

Figure 6 Effects of the rolling friction coefficient α on peak dilation angle (a) as function of friction coefficient μ and (b) vertical normal stress σ_1

4.3 Effect of Rolling Resistance on Shear Band Orientation

To further quantify the effects of rolling resistance on shear band formation, the orientations of the shear bands were directly measured from the models. Only the cases with distinctly observable shear bands were included in the analysis. It was observed that the shear bands were not always completely straight along its length, but sometimes tend to bend towards the corners of the four edges of the samples. Thus, the shear bands were measured along the straight line portions of the shear bands in the middle of sample. The orientations of the shear band plane θ_m from the models were measured from the horizontal axis, and these are shown against α in Fig. 7. The measured shear band inclinations are compared with three theoretical shear band orientations. These are the Mohr-Coulomb orientation θ_{MC} and Roscoe orientation θ_R [9] which is, respectively, the upper and lower bound values of the orientation of the shear band plane measured from the horizontal axis (Eqs. 3 and 4). The third orientation is the Arthur-Vardoulakis orientation θ_{AV} from [10, 11] which corresponds to the average inclination between the Mohr-Coulomb and Roscoe orientations (Eq. 5). Figure .7 shows the variation of the measured shear band orientation θ_m from the models against the rolling friction coefficientα. It is observed that θ_m first increases with increasing value of α. The measured shear band inclination angle for free rotation is about $\theta_m = 55^O$, then it reaches its highest value at about $\theta_m = 58^O$ at α=0.1 and decreases thereafter to $\theta_m = 57^O$ for α=1.0.

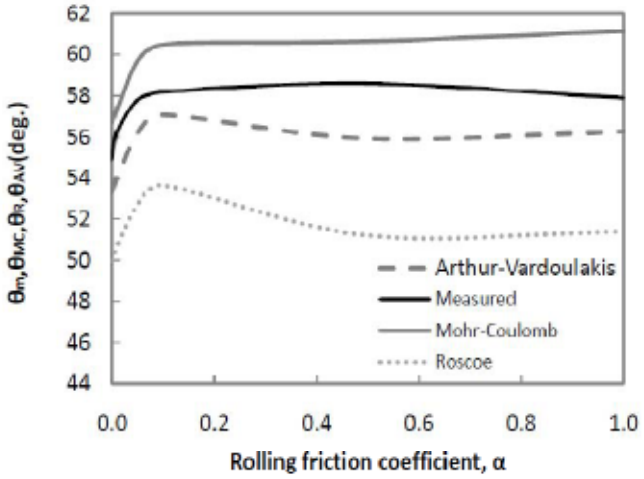

Figure 7 Effects of the rolling friction coefficient α on shear band orientation

Figure 7 also shows the Mohr-Coulomb, Roscoe and Arthur-Vardoulakis shear band orientations from Eqs. 4 and 5 using the measured peak friction angle $\emptyset$ and dilation angle φ from the models. The measured shear band orientations are located between the Arthur-Vardoulakis and Mohr-Coulomb orientation predictions. The Mohr-Coulomb orientation over predicts while the Arthur-Vardoulakis orientation under predicts the measured shear band inclinations. Similar variation of shear band orientation as function of α, were observed for different particle sizes and values of the friction coefficient μ and confining stress σ_3.

4.5 Micromechanical Observations

One of interesting features that arise from micromechanics analysis is the formation of force chains which are considered the primary load carrying mechanism of granular materials [10], where the contact force between them is rather stronger than the other force outside particle chains. Force chains are quasilinear arrangements of groups of particles by which almost all the shear loads are transmitted. Their average orientations are more or less sub-parallel to the major principal stress, and they form solid column-like structures in order to resist the shear stress and insure stability of granular materials. When a granular assembly is loaded and sheared, force chains form, rotate and collapse as the shearing progresses. Force chains develop anisotropically during shearing due the fact that not all particles are selected to form force chains. As the shearing proceeds beyond peak shear stress, the major force chains reorganize until they can no longer provide the best possible set of stress pathways for force transmission.

The reconfiguration of force chain networks for granular assembly subjected to simple shear loading is associated with the rotation of principal stress. The direction of force chain is consistent with the rotated stresses. Before shear loading, the network of force chains is dense and evenly distributed with no preferred directions throughout the volume of the granular materials (see Fig. 8a). Once the granular assembly is loaded, all pathways can be developed into strong and weak force chains as they formed to transmit the shearing loading. The key feature of simple shear condition during shearing is associated with the principal stress rotation. Therefore, the microstructure of force chains undergoes sub parallel with the rotated

principal stresses (see Fig. 8b). Once the peak shear stress is reached, the density of the number of force chains is reduced inside the shear band, and there are fewer particle-to-particle contacts available within the shear band to transmit the loads.

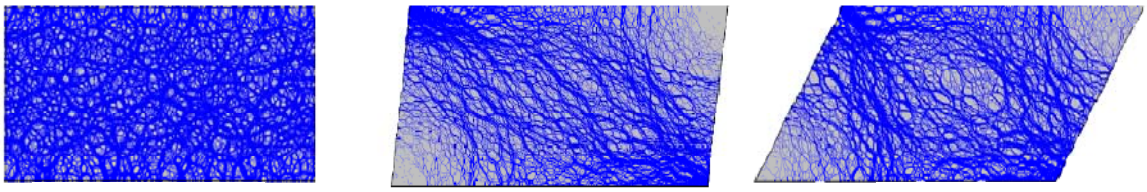

(a) ε_1=0.0% (b) ε_1=12% (c) ε_1=50%

Figure 8 Development of force chains at different levels of axial strain (α=0.2).

As the number of particle contacts is decreased, the shear loading may exceed the frictional resistance between particles causing the force chain to collapse, limitation of force chain collapsing leads localization of strain (see Fig. 8c). As the shearing proceeds beyond peak shear stress, shearing process leads to the exhaustion of the strength of the material. As a result, the load carrying capacity of granular materials is reduced and strain softening occurs [12]. Due to the deviation of the force chain directions from the major principal stress direction, high rotational moments and stress gradients were produced within the shear band. Instability and strain localization occurred due to the changes in configuration of the force chains and the presence of rotational moments and stress gradients. In the case of α=0, particles rotated widely over the granular assembly at all stages of deformation. In comparison, in the case of rolling resistance, the particles showed only very small rotations before the shear band was formed.

Once deformations have localized, particle rotation occurred extensively within the shear band while no significant rotations were observed for the particles outside the shear band. As a result, the shear band formation was accompanied by gradients in the magnitude of particle rotations. Particle rotation within the shear band in the presence of rolling resistance was associated with the formation of non-uniform void distribution within the shear band. Paradoxically, large voids were created at the same time that the shear band width decreased as α is increased. The occurrence of areas of large voids where particles have high rolling resistance was attributed to the fact that particles, in the presence of rotational moments, tended to push each other apart. This caused the granular assembly to expand and increase the porosity locally. In comparison, particles were free to move and accommodate each other, resulting in more uniform void distribution.

4.6 Strain Localization inside the Shear Band

The development of strain localization can be better evaluated by the shear strain contours show in Fig. 9. The shear strain e_{ij} value is calculated using the proposed strain calculation method (Eq. 2), using the mesh-free method. A series of micro bands emerge in a sequential way to form the final shear band. Results show that the shearing condition inside the granular specimen during initial conditions is assumed to be uniform. Hence, there is not any sign of strain localization existence (Fig. 9a). As shearing proceeds, some shear distortion has occurred at pre failure γ_{xy}=0.13, indicating the plastic shear band extends over the length at the

middle plane propagating straight in the horizontal direction. Meanwhile, nonlinear stress-strain behavior marks the effective start of plastic regime and the onset of shear band would become. The shear band in this stage cannot be seen clearly in Fig. 9b due to the resolution of the plot. A fairly small and uniform strain field can be found inside granular assembly as a plastic flow confined between two semi-rigid plates moving in opposition directions. After peak state, the shear band expands and becomes expansive and coherent with post peak strain softening immediately after failure γ_{xy}=0.16. The peak of the mound is located approximately at the middle of the shear box, with a width of about 18 median particle diameters thick (Fig. 9c). During the processes of strain localization, not only the shear strain increases but also the volumetric strain is locally increased due to localized dilatancy. At steady state γ_{xy}=0.38, a distinct shear band is observed which becomes continuous, cumulative and thicker, dividing the shear box into two halves. However, the contour plot clearly shows that the strain localization is fully developed (Fig. 9d). The thickness of the strain localization zone was almost 10-20 times the median particle diameter D_{50} on the average and increase generally with increasing of shear strain. The increase in dilation is attributed to the increase of the interface between particles and the subsequent increase in the shear band thickness.

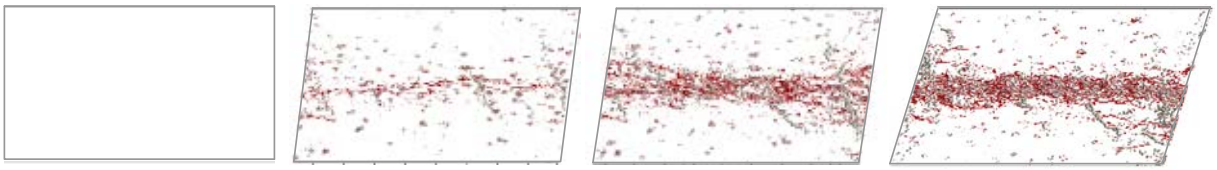

Figure 9 Shear band formations inside dense sample corresponding simple shear loading.

5 CONCLUSIONS

This work presents an extensive investigation of the effects of rolling resistance on macro behavior of granular specimens subjected to simple shear loading conditions using DEM modeling. The Modified DEM implemented a rolling resistance model in PFC. The results concluded that the Young's modulus *E* and Poisson's ratio ν were relatively unaffected by the rolling friction coefficientα. The peak secant friction and dilation angles increased with increasing value of the rolling friction coefficientα. Once deformations have localized, particle rotation occurred extensively within the shear band while no significant rotations were observed for the particles outside the shear band. Particle rotation within the shear band in the presence of rolling resistance was associated with the formation of non-uniform void distribution within the shear band. The shear strain contours developed using the mesh-free method, indicating that strain localization does not exist during initial conditions. As shearing proceeds, the shear band thickness expanded and became thicker and generally increased with increasing shear strain. This observation is attributed to the increase in local softening and dilation inside shear localization zone.

REFERENCES

[1] Mohamed, A.M. and Gutierrez, M. Comprehensive study of the effects of rolling resistance on the stress–strain and strain localization behavior of granular materials, *Gran. Matter* (2010)**12**(5): 527–541.

[2] Iwashita, K., Oda, M. Micro-deformation mechanism of shear banding process based on Modified Distinct Element Method. *Powder Tech* (2000)**109:**192-205.

[3] Itasca Consulting Group: Particle Flow Code in 2D (PFC-2D): User's Manual, Version 4.0. Minneapolis, Minnesota (2008).

[4] Ng, T.T. Input parameters of discrete element methods. *J. Eng. Mech* (2006)**132**(7):723-729.

[5] Wang, J.**,** Dove, J.E. and Gutierrez, M.S. Discrete-Continuum Analysis of Shear Band in the Direct Shear Test, *Géotechnique* (2007)**57**(6): 527-536

[6] Bardet, J.P. Observations on the effects of particle rotations on the failure of idealized granular materials. *Mech. Matls* (1994)**18:**159-182.

[7] Wang, J.F., Gutierrez, M., Dove, J.E. Effect of particle rolling resistance on interface shear behavior. *Proc. 17th ASCE Eng. Mech. Conf* (2004):56–63.

[8] Tordesillas, A. Force chain buckles, unjamming transitions and shear banding in dense granular materials. *Phil. Magng* (2007) **87:** 4987–5016.

[9] Roscoe, K.H. The influence of strain in soil mechanics. *Géotechnique* (1970) **20**(2):129-170.

[10] Arthur, J., Dunstan, T., Al-Ani, Q., Assadi, A. Plastic deformation and failure in granular media. *Geotechnique* (1977)**27**(1):53-74.

[11] Vardoulakis, I. Shear band inclination and shear modulus of sand in biaxial tests. *Int. J. Num. Anal. Methods. Geomech* (1980)**4**(2):103-119.

[12] Tordesillas, A., Peters, J. F., Muthuswamy, M. Role of particle rotations and rolling resistance in a semi-infinite particulate solid indented by a rigid flat punch. *The ANZIAM J.* (2005)**46:** 260-275.